A case of anomalous electric field perturbations in the equatorial ionosphere during post-sunset hours: insights

A. Kumar[1,2], D. Chakrabarty[1], B.G. Fejer[3], G.D. Reeves[4], D. Rout[5], S. Sripathi[6], G. K. Seemala[6], S. Sunda[7], A. K. Yadav[1]

[1]Physical Research Laboratory, Ahmedabad, India
[2]Indian Institute of Technology, Gandhinagar, India
[3]Utah State University, Logan, UT, USA
[4]Space Science and Applications Group, Los Alamos National Laboratory, Los Alamos, NM, USA
[5]GFZ German Research Centre for Geosciences, Potsdam, Germany
[6]Indian Institute of Geomagnetism, Navi Mumbai, India
[7]Airport Authority of India, Ahmedabad, India

Key Points:

- Under southward IMF Bz conditions, anomalous electric field perturbations are observed over the equatorial ionosphere.
- The amplitude of electric field perturbations are more when the magnitude of IEFy is less and vice-versa.
- These anomalous electric field perturbations are explained based on the effects of IMF By and substorm.

Corresponding author: Ankit Kumar, `ankitprl2017@gmail.com`

This article has been accepted for publication and undergone full peer review but has not been through the copyediting, typesetting, pagination and proofreading process, which may lead to differences between this version and the Version of Record. Please cite this article as doi: 10.1029/2022JA030826.

Abstract

During a weak geomagnetic storm (Ap = 15) on 24 December 2014, the penetration electric field perturbations over the Indian dip equatorial sector are found to be anomalous on a number of occasions during post-sunset hours. The event is anomalous as the magnitude and polarity of penetration electric fields do not obey the existing paradigm. The penetration electric field perturbations are investigated using the vertical drifts derived from the CADI (Canadian Advanced Digital Ionosonde) measurements at Tirunelveli (8.7° N, 77.7° E, dip angle: 1.7°). During this event, we observed post-sunset vertical drift of $\sim$ 42 ms^{-1} not only at 1810 LT but also $\sim$ 36 ms^{-1} at $\sim$ 2100 LT which is anomalous. Interestingly, the dawn-dusk component of interplanetary electric field (IEFy) is relatively less (< 2 mV/m) at $\sim$ 2100 LT compared to the interval 1930-2030 LT (IEFy $\sim$ 3 mV/m). Despite that, the vertical drift observed over Tirunelveli is very close to zero or nominally upward during 1930-2030 LT. In addition, the downward drift just after 2130 LT on this night is found to be exceptionally large ($\sim$-60 ms^{-1}). By combining vertical total electron content over the Indian sector with the OI 630.0 nm airglow intensity from Mt. Abu, chain of magnetometer and Los Alamos National Laboratory (LANL) geosynchronous satellite particle measurements, it is suggested that the anomalous penetration electric field perturbations on this night arise from the effects of IMF By and substorm.

Plain Language Summary

Variation in the zonal electric field in the equatorial ionosphere during post-sunset hours is important to understand the plasma distribution over low latitudes and also generation of plasma irregularities. The changes in the ionospheric conditions over low/equatorial latitudes have implications for communication and navigational applications. Therefore, if ionospheric electric field over equatorial ionosphere behaves anomalously during space weather events, it will be difficult to model the low latitude ionopshere for scientific understanding and practical applications. In this investigation, we show that the less studied Y-component of interplanetary magnetic field and substorm can significantly modulate the ionospheric electric field giving rise to anomalous response.

1 Introduction

The F region vertical drifts are upward in the daytime and downward in the night time during geomagnetically quiet periods (e.g., Fejer et al., 2008a). However, the equatorial F region vertical drifts can be enhanced or reduced under the influence of space weather related perturbation electric fields. It is known that the southward directed IMF Bz drives geomagnetic storm and during a storm, the Y- component (Dawn-Dusk direction) of solar wind/interplanetary motional electric field (IEFy) maps down to the polar ionosphere. This electric field drives a two-cell ionospheric plasma convection pattern or disturbance Polar type 2 or DP2 cells (e.g., Nishida, 1968). During this period, region 1 Field aligned current (R1 FAC) develops rapidly and region 2 field aligned current (R2 FAC) takes time to develop as it is sluggish in nature compared to R1 FAC. Owing to the different time constants of R1 and R2 FACs, the convection electric field perturbations penetrate to the low latitude ionosphere through the polar ionosphere. This is known as prompt penetration electric field (PPEF). In an equivalent description, this happens under undershielding condition when the shielding electric field in the inner magnetosphere is not fully developed in response to the convection electric field imposed at the outer magnetosphere. Earlier studies (e.g., Fejer et al., 2008b) reveal that PPEF generates eastward/westward electric field perturbations in the equatorial ionosphere during daytime/nighttime. On the contrary, when IMF Bz suddenly turns northward from southward condition, R1 FAC decays quickly compared to R2 FAC and the residual shielding electric field survives in the inner magnetosphere for some time. It is this residual electric field that has the opposite polarity of PPEF (e.g., Kikuchi et al., 2008). This is known as the overshielding effect and the electric field perturbations experienced in the inner magnetosphere/ionosphere during this time is commonly termed as overshielding electric field. The impact of PPEF over low and equatorial ionosphere has been reported observationally (e.g., Chakrabarty et al., 2005, 2008, 2015; Tsurutani et al., 2008) and studied through simulation (e.g., W. Wang et al., 2008; Lu et al., 2012). During PRE-hours, significant effects of PPEF over the dip equatorial ionosphere have been studied by several researchers (e.g., Rout et al., 2019; Abdu et al., 2018; Fejer et al., 2021; Tsurutani et al., 2008) in the past. The role of PPEF in generating ionospheric super fountain (e.g., Tsurutani et al., 2004; Mannucci et al., 2005) over the low latitude and latitudinal expansion of the equatorial ionization anomaly, (EIA) crest toward higher latitudes (e.g., Rout et al., 2019) have also been shown. Rout et al. (2019) studied the largest PRE-associated vertical drift ($\sim 150\ ms^{-1}$) over Jicamarca during a space weather event in September 2017. They also brought out latitudinal expansion of the EIA crest along the 75°W longitude. The modeling (e.g., Nopper Jr. & Carovillano, 1978) and observational (e.g., Fejer et al., 2008b) studies also suggest that the eastward perturbations of PPEF is expected till 2200 LT. Further, it is also shown that 6-9% of IEFy penetrates to the equatorial/low latitude ionosphere (e.g., Kelley et al., 2003; Huang et al., 2007). Significantly large PPEF can change the plasma distribution over low latitudes during daytime and post-sunset hours (e.g., Tsurutani et al., 2008; Balan et al., 2009, 2018; Abdu et al., 2018; Rout et al., 2019) substantially and can shift the location and strength of the EIA crest over low latitudes.

In addition to storm, magnetospheric susbtorms can also generate transient electric field disturbances (e.g., Kikuchi et al., 2000, 2003; Huang et al., 2004; Huang, 2009; Chakrabarty et al., 2008, 2010, 2015) over low latitude ionosphere. Substorms are magnetosphere's way of unloading excess energies stored during the re-organization of the magnetic flux in the magnetotail. Substorms can be directly triggered by the changes in the solar wind parameters like IMF Bz flipping from southward to northward suddenly, abrupt changes in the solar wind dynamic pressure etc. (e.g., McPherron, 1979; Lyons, 1995, 1996; Lyons et al., 1997) or can be spontaneously triggered (e.g., Angelopoulos et al., 1996; Henderson et al., 1996) wherein clear solar wind triggering is not obvious. The spontaneously triggered substorms are believed to be triggered by internal magnetospheric processes or by the self organized criticality (e.g., Baker et al., 1997; Klimas et al., 2000; Tsurutani et al., 2004) of the plasma sheet. Substorms are nightside, longitudinally confined phenomena. Although the substorm induced electric fields are experienced over low latitude ionosphere during nighttime (e.g., Chakrabarty et al., 2015), the dayside electric field perturbations in the low latitude ionosphere due to substorms are also not uncommon (e.g., Kikuchi et al., 2003; Huang, 2009; Hashimoto et al., 2017; H. Wang et al., 2019). Moreover, substorms can exert both eastward (e.g., Huang, 2009; Chakrabarty et al., 2010; Hui et al., 2017) and westward (e.g., Kikuchi et al., 2003; Chakrabarty et al., 2015; Hashimoto et al., 2017; Hui et al., 2017) electric field perturbations over low latitude ionosphere. Therefore, simultaneous presence of substorms can augment or annul the prompt electric field perturbations arising out of undershielding/overshielding effects as shown in a few earlier studies (e.g., Hui et al., 2017; Rout et al., 2019). In addition to the above processes, sudden changes in the solar wind dynamic pressure can also lead to changes in the Chapman Ferraro current and cause prompt electric field disturbances (e.g., Sastri et al., 1993; Huang et al., 2008; Rout et al., 2016) over equatorial ionosphere. In recent times, it is also unambiguously brought out that the effects of IMF By can also change the expected polarity of electric field perturbation (e.g., Chakrabarty et al., 2017) over equatorial ionosphere particularly during the post-sunset hours.

Therefore, under disturbed space weather conditions, some of the prompt electric field disturbances can occur simultaneously and can reinforce or annul individual effects making the phenomenological understanding of the equatorial impact difficult (e.g., Chakrabarty et al., 2015; Hui et al., 2017; Rout et al., 2019). In addition, these prompt electric field perturbations can also compete with the delayed electric field perturbations owing to what is known as disturbance dynamo mechanism (e.g., Blanc & Richmond, 1980) associated with the altered circulations of thermospheric wind systems following storm and substorm. Therefore, understanding the origin of prompt electric field perturbations over low-equatorial ionosphere deserves further investigation. In this regard, those cases are particularly important wherein the magnitude and polarity of penetration electric field in the equatorial ionosphere do not follow the existing understanding. The present investigation is important as it brings out such a case and shows that the phenomenological origin of the prompt penetration electric field perturbations over the low latitude ionosphere is more complex than what is believed.

2 Datasets and methodology

1-minute cadence data of the solar wind parameters like interplanetary magnetic field (IMF), solar wind velocity, dynamic pressure and density are obtained from space physics data facility (SPDF) of Goddard Space Flight Center (https://cdaweb.gsfc.nasa.gov/). It is to be noted that the solar wind data available at this site are already time-shifted to the nose of the bow shock. In order to evaluate the ionospheric impacts, the magnetosheath and alfven transit times are calculated and added to the lag time, point by point, following the methodology reported in Chakrabarty et al. (2005). In addition, symmetric ring current (Sym-H) index, auroral electrojet (AE) index and polar cap (PC) index are also taken from SPDF.

In the absence of incoherent scatter radar over the Indian sector, the nighttime F region vertical drift over the Indian dip equator is derived by taking the temporal derivative of the bottom-side F layer height ($h'F$). The $h'F$ values are obtained from the CADI over Tirunelveli (8.7°N, 77.7°E, dip angle: 1.7°). The details of the CADI system are described by MacDougall et al. (1995) and Sripathi et al. (2016). As the CADI data is slightly noisy, the h'F is smoothed with the Savitzky-Golay (SG) algorithm (e.g., Savitzky & Golay, 1964) with 15% smoothing window. The advantage of SG algorithm lies in it's ability to suppress the noise in the data without introducing any significant distortion. Subsequently, temporal derivative of $h'F$ ($dh'F/dt$) is calculated. It is to be noted that below 300 km altitude, the recombination process can also introduce an apparent upward drift as pointed out by Bittencourt and Abdu (1981). Therefore, in order to obtain the actual electrodynamical vertical drift, the apparent upward drift due to chemical recombination needs to be corrected. βH values are subtracted from $dh'F/dt$ to get the corrected vertical drift where β and H are the attachment coefficient and the scale height of plasma respectively. β is calculated by the following formula, $\beta = K_1[O_2] + K_2[N_2]$. Where K_1, K_2 and $[O_2]$, $[N_2]$ are the reaction rate coefficients and molecular density of oxygen, nitrogen respectively. H is calculated by the following formula $\frac{1}{H} = \frac{1}{n}\frac{\partial n}{\partial h}$, where n and h are the plasma density and height from the earth's surface. The parameters K_1 and K_2 are taken from Anderson and Rusch (1980). The neutral parameters, e.g., molecular densities and thermospheric temperature, are taken from the NRLMSIS 2.0 (Emmert et al., 2021). For the present investigation, the typical scale height is calculated corresponding to 2100 LT on a quiet (28 November 2014) and the event day (24 December 2014) to calculate the recombination- corrected vertical drifts wherever applicable. Typical β is also calculated at 2100 LT (from 100 to 600 km in steps of 5 km). The typical uncertainty in the drifts derived based on ionosonde measurements is of the order of 10% (e.g., Woodman et al., 2006).

In order to get an idea about the daytime ionospheric electric field behaviour, the equatorial electrojet (EEJ) strength is derived over both the Indian and Peruvian sectors. Over the Indian sector (e.g., Rastogi & Patel, 1975), EEJ strength is calculated using the systematic measurements of horizontal component (H) of geomagnetic field from a dip equatorial station, Tirunelveli (TIR) and the off-equatorial station, Alibag (ABG, 18.6°N, 72.9°E, dip angle: 26.4°). EEJ is calculated using the following formula, $EEJ_{India} =$

ΔH_{TIR} – $-\Delta H_{ABG}$. Here, ΔH is the instantaneous value of H corrected for the nighttime (during 2300 – 0300 LT) average quiet base values of H. The temporal cadence of EEJ data is 1 min. The EEJ strength over the Peruvian sector is, in general, derived by taking magnetometer data over the equatorial station, e.g., Jicamarca (JIC, 11.5°S, 76.5°W, dip angle: 1.0°), and off-equatorial station, Piura (PIU, 5.2°S, 80.6°W, dip angle: 12.5°) (e.g., Rastogi & Klobuchar, 1990). As the magnetometer data over Piura is not available during the event under consideration here, data from another off-equatorial station, Leticia (LET, 4.2°S, 70.0°W, dip angle: 12.6°) is used in place of Piura. The local time of Leticia is also appropriately corrected to take account for the longitudinal difference between Jicamarca and Leticia and the resultant EEJ strength corresponds to the local time of Jiamarca. 1-minute cadence data of both magnetometer stations are used to derive EEJ strength over the Peruvian sector by the following formula, $EEJ_{Peru} = \Delta H_{JIC} - -\Delta H_{LET}$.

Magnetometer data from a set of nearly antipodal stations (nearly 12 hours difference in the local time of the given set of stations with nearly similar latitudes) along the Indian and Peruvian longitudes are also used in this work to understand the variations of DP2 currents over the two sectors. This is done following the methodology suggested in Chakrabarty et al. (2017). In this work, the important role of this approach in identifying the role of IMF By is pointed out. During the event under consideration, India is in the post-sunset to pre-midnight sector while Peru is in the morning sector. The northward component of magnetic field, ΔX (ΔX is the instantaneous value corrected for the quiet nighttime base values), for stations is obtained from the SuperMAG worldwide network (https://supermag.jhuapl.edu/). For the present work, magnetometer stations along Indian (145°E-177°E) and Jicamarca (3°W-20°W) longitudes are Novosibirsk (NVS, 45.8°N, 159.9° E) and Ottawa (OTT, 54.9°N, 3.8°W); Irkutsk (IRT, 42.4°N, 177.4°E) and Fredericksburg (FRD, 47.8°N, 5.8°W); Alma Ata (AAA, 34.5°N, 153.1°E) and Bay St Louis (BSL, 39.4°N, 18.9°W); Tirunelveli (TIR, 0.18°N, 150.7°E) and Huancayo (HUA, 2.2°S, 2.6°W) as well as Alibag (ABG, 10.4°N, 146.8°E). 1-minute cadence data are used for all the stations.

In order to assess the effects of disturbance dynamo (DD) on 24 December 2014, we estimate magnetic disturbance in H- component (D_{dyn}) using an established methodology (e.g., Zaka et al., 2009; Amory-Mazaudier et al., 2017; Pandey et al., 2018; Rout et al., 2019).

$$D_{dyn} = \Delta H - S_R - SymH \times cos(L) \tag{1}$$

In Equation 1, ΔH and S_R are the event day and quiet time average magnetic field variations above the crustal magnetic field values. $SymH$ is the strength of the ring current. L is the magnetic latitude at that station where the magnetic disturbance (D_{dyn}) is calculated. As the H variation due to ionospheric current is unambiguous during daytime, the magnetometer data between the geographic longitudes 275°-300°E which is in day sector during the event under consideration, have been used to calculate D_{dyn} in this work. D_{dyn} is calculated over the stations, Vernadsky (AIA, 55.4°S, 6.1°E), Trelew (TRW, 33.4°S, 6.24°E), Pilar (PIL, 21.8°S, 7.9°E), Huancayo (HUA, 2.2°S, 2.7°S), San Juan (SJG, 27.7°N, 6.8°E), Ottawa (OTT, 54.9°N, 3.7°W), Iqaluit (IQA, 73.3°N, 6.2°E), and Thule (THL, 87.1°N, 14.2°E). These data are obtained from the INTERMAGNET network (https://www.intermagnet.org/index-eng.php).

The present investigation requires identification of the substorm induced electric field perturbations over the low latitude ionosphere. We identify substorms using observations of dispersionless injection of energetic particles (electrons and protons) at the geosynchronous orbit (e.g., Reeves et al., 2003). This is considered to be one of the telltale signatures of the onset of substorms (e.g., Reeves et al., 2003). The data from Los Alamos National Laboratory (LANL) -01A, 02A, 04A, 97A, 080, and 084 geosynchronous satellites are used for the present study. The electron and proton flux data are taken from all these satellites for the event day from 1200 to 1900 UT (universal time).

To understand the low latitude plasma distribution over the Indian sector, and the approximate location of the EIA crest and its strength, the measurements of total electron content (TEC) by the Indian Satellite-based Augmentation System (SBAS) is used. Indian SBAS network is known as GAGAN (GPS Aided Geo Augmented Navigation). As part of GAGAN, 5 minutes cadence of SBAS-TEC data is available at 102 ionospheric grid points over the Indian sector. The data of these grid points are generated by using 13 ground stations. The details of GAGAN SBAS-system are described by Sunda et al. (2015).

OI 630.0 nm airglow intensity over Mt. Abu (24.6°N, 72.7°E, dip angle: 38.0°), a station typically under the crest of EIA, is used for the present study. 10-sec cadence airglow intensity data was captured by a narrow spectral band (bandwidth 0.3 nm) and narrow field-of-view (3°) airglow photometer in a campaign mode in cloudless and moonless conditions during December 2014. The details of this photometer are available in the literature (e.g., Chakrabarty et al., 2008, 2015; Sekar & Chakrabarty, 2011). Note, the instrumental parameters remains the same during the campaign and hence, despite absolute airglow intensity levels (in Rayleigh) are not being known during the nights under this campaign, gross comparison of the night to night changes in the peak intensity levels during the campaign can be made.

Slant total electron content (STEC) is measured over Ahmedabad (23.0°N, 72.6°E, dip angle: 35.2°) by a dual-frequency (L-band, 1575 and 1227 MHz) GPS receiver (GISTM GSV4004B) at the Physical Research Laboratory (PRL). Vertical TEC (VTEC) is derived from STEC using a standard methodology described in Manke and Chakarabarty (2016). For the present work, ray path elevation angle of less than 30° is not considered to minimize the multipath error and tropospheric effects. 5 minutes cadence VTEC data is used in this case study. It is to be noted that, local time over Indian longitude is taken along 75°E longitudes (LT = UT + 5 hrs) in present investigation.

3 Results

Figure 1 depicts the variations of a few interplanetary (Figures 1a-d) and ground-based parameters (Figures 1e-f) from 21 to 25 December 2014. The Ap values for these days are 12, 19, 11, 15, and 11 respectively. In Figure 1 (from top to bottom), IMF Bx (in nT), IMF Bz (in nT), solar wind velocity (in kms^{-1}), IMF $|B|$ (in nT), Sym-H (in nT) and $h'F$ (in km) are shown in black lines while IMF By (in nT), IEFy (in mV/m), solar wind density (cm^{-3}), solar wind pressure (nPa), EEJ_{India} (in nT) and OI 630.0 nm airglow intensity (in arbitrary units) are depicted in red lines. The Y-axes corresponding to black and red lines are marked on the left and right side of Figure 1. It can be clearly noticed from Figure 1 that the peak $h'F$ and 630.0 nm airglow intensity are higher in the local night of 24 December, 2014 in comparison with the rest of the nights shown in Figure 1. This is despite IMF Bz being more southward for some time on 22 December (pre-noon hours over the Indian sector) and 23 December (pre-midnight hours over the Indian sector) compared to the interval of interest on 24 December, 2014. In fact, the characteristically different variation in OI 630.0 nm airglow intensity on this night motivated us to pursue this investigation.

Figure 2 shows observations on 24 December 2014 along with observations from a quiet day (28 November 2014) for comparison. Note, the daily mean Ap is 3 on 28 November, 2014 and 7 on the previous day. In all the panels, the quiet and disturbed variations are shown with blue and red colored lines respectively. Figure 2a depicts the derived vertical drift variations over Tirunelveli (red) on the event day along with the vertical drift variations on the quiet day (blue). The vertical drift variation during post-sunset hours is found to deviate from the variation on the quiet day. It can be seen that pre-reversal enhancement (PRE) of equatorial zonal electric field is enhanced on the event day (24 December, 2014). The vertical drift corresponding to PRE occurs at $\sim$ 1310 UT (1810 LT) on the event day with an amplitude of $\sim$ 42 ms^{-1}, which is higher than PRE amplitude on a quiet day ($\sim$ 25 ms^{-1}). More importantly, although the vertical drift decreases after the PRE hours, drift does not turn steadily downward on the event night compared to what happens on a quiet day. It can be noted that vertical drift turns downward during 1400-1430 UT (1900-1930 LT) on a quiet day. In sharp contrast to a quite day variation, the vertical drift again starts increasing from 1500 UT (2000 LT) on 24 December, 2014 and another peak in vertical drift occurs at $\sim$ 1600 UT (2100 LT) with an amplitude of $\sim$ 36 ms^{-1} on the event night. Note that the vertical drift at this local time is expected to be significantly downward as indicated by the quiet time reference drift. Further, the vertical drift is found to be minimum ($\sim$-60 ms^{-1}) at $\sim$ 1640 UT (2140 LT) which is significantly higher than the corresponding downward drift ($\sim$-15 ms^{-1}) during a quiet night at this local time. The vertical drift again starts decreasing just before 1700 UT (2200 LT) and becomes less downward at 1730 UT (2230 LT) to match with the corresponding quiet time drifts afterwards.

Figure 2b shows vertical total electron content variation over Ahmedabad on 24 Decmber, 2014 (red) and 28 November, 2014 (blue) respectively. The figure reveals that the post-sunset enhancement in VTEC over Ahmedabad is higher and sustains for a longer period on the event day than on the quiet day. In Figure 2c, variations in OI 630.0 nm airglow intensity over Mt. Abu on the event day (red) shows different temporal pattern than what is noticed on the control day (blue). The intensity variation on the event night is characterized by three enhancements peaking at 1445, 1600, and 1640 UT (1945, 2100 and 2140 LT). In fact, the late enhancements at 1600 UT and 1640 UT are in sharp contrast with the monotonic decrease in intensity found on the control night at this local time.

Figure 2d is constructed with the help of SBAS-TEC data that shows the local time variations of TEC over the EIA crest location. The event and control days are marked by red and blue lines respectively. On both days, the crest location is found either closer to 7.5°N (solid line with star) or 12.5° (solid line) magnetic latitudes during post-sunset hours. One can notice in Figure 2d that the EIA crest is located at 12.5°N till 1730 UT (2230 LT) on event day, whereas on the quiet day, the EIA crest is observed at 12.5°N magnetic latitudes till 1515 UT (2015 LT). After this, the location of the EIA crest is found at 7.5°N.

Figure 3 is dedicated to identify the anomalous vertical drift variations on the event night (24 December 2014). Figure 3a is a replica of Figure 2a and is presented again for continuity. The variations in EEJ strength over Jicamarca for the event day (in red) and quiet day (in blue) are depicted in Figure 3b. In Figure 3c, the variations in ΔVd over Tirunelveli (red) and ΔEEJ over Jicamarca (black) are shown. The ΔVd and ΔEEJ are derived by subtracting the vertical drift and EEJ strength of the quiet day from their event day counterparts. Figures 3d-3f depict the variations of a few interplanetary parameters (IMF Bz, IEFy and IMF By) and geomagnetic indices (AE and PC) on the event day only. Figure 3d represents the variations in IMF Bz (in black) and IEFy (in red). Variations in IMF By are shown in Figure 3e. Figure 3f depicts the variations in Auroral electrojet (AE) and polar cap (PC) indices. A few vertically shaded (in orange and green colors) intervals (marked by Roman numbers I-V) are overlaid at appropriate places in Figures 3a-3e to bring out the important features that emerge out of this set of observations. The criterion for the divisions of the intervals is based on the conspicuous differences of the vertical drift variations on the event night with reference to the quiet night. The interval-I shows that the vertical drift in event night is conspicuously more than the quiet night. On the other hand, interval-II highlights the onset of departures of the vertical drift polarity with respect to the quiet night. Interval-III captures significantly anomalous electric field perturbations with opposite polarity. Interval-IV captures much larger downward drift on the event night than what is expected during a quiet night at this local time. Lastly, during interval-V, the vertical drift on the event night recovers and catches up with the corresponding variations during the quiet night. In addition, two simultaneous peaks in AE and PC indices around 1415 UT (1915 LT) and 1630 UT (2130 LT) are shown by gray and brown shaded boxes. In Figure 3d, the dashed blue lines are used to guide the eye towards the net decrease in southward IMF Bz and IEFy respectively during the period ∼1400-1600 UT (1900-2100 LT). In the ensuing paragraphs, we highlight the important observational features of interval-I-V.

Interval-I: During interval-I (∼1250-1330 UT, LT are shown at the top of the Figure), IMF Bz is southward, and vertical drift is upward with an amplitude of $\sim 42\ ms^{-1}$. This drift is more than the quiet time drift ($\sim 25\ ms^{-1}$) even if one considers 10% uncertainty in the vertical drift. Therefore, the enhanced PRE drift at this interval is due to the penetration of IEFy to equatorial ionosphere and this change is noticed $\sim 17\ ms^{-1}$.

Interval-II: In the course of interval II (∼1420-1530 UT), southward IMF Bz decreases (from ∼-6 nT to -1 nT) leading to the decrease in IEFy. IEFy changes to +0.5 mv/m from +3 mV/m during this interval. However, equatorial vertical drifts remain close to zero for some period and then enhances with net decrease in the magnitude of IEFy. Note, IMF By oscillates with a sharp negative excursion sandwiched between two positive excursions during this interval. Further, strong enhancements in AE (reaches ∼ 900 nT) and PC indices are observed during this interval apparently suggesting occurrence of susbtorm. However, Figure 4 would subsequently confirm that the enhancement of AE and PC indices at this local time ∼ 1915 LT (1415 UT) are not due to substorm induced electric field perturbations but possibly due to enhancement in polar cap electric field at this time due to enhanced IEFy. Another important aspect emerges from Figure 3c shows the polarity of both ΔVd and ΔEEJ derived based on Figure 3a and 3b respectively, is positive.

Interval-III: During interval-III (∼1530-1615 UT), IMF By changes polarity from negative to positive. Net IMF Bz (dashed line in blue) is less southward than interval-II. However, vertical drift keeps increasing with a maximum amplitude of $\sim 36\ ms^{-1}$ at 1550 UT (2050 LT). Note, the maximum vertical drift during this interval is nearly comparable to PRE-associated vertical drift during post-sunset hours. Although IMF By turns positive (similar to interval-II) during this interval, ΔVd and ΔEEJ are opposite unlike interval-II (Figure 3c).

Interval-IV: Interval-IV (∼1630-1700 UT) is characterized by highest downward drift amplitude ($\sim$-62 ms^{-1}) at ∼ 1640 UT (2140 LT) on the event day. This is significantly different than the quiet day drift ($\sim$-15 ms^{-1}) at this local time. During this interval, IMF Bz is southward and the amplitude is similar to interval-II. In addition, IMF By is initially negative and then sharply turns to positive direction. Considering 10% efficiency of the penetration electric field reaching to the dip equator, the difference in the observed and expected drifts $\sim 48\ ms^{-1}$ (Figure 3c) cannot be explained even after considering a typical 10% uncertainty in the drift. In addition, enhancements in AE and PC indices are seen during this interval (peak ∼ 1630 UT) although these enhancements are less compared to the enhancements in these indices seen around 1415 UT. Based on Figure 4, it is confirmed subsequently that the enhancement of AE and PC indices at this local time (∼ 2130 LT) are due to additional effects of substorm induced electric field perturbations. Further, similar to interval-III, the polarity of the electric field perturbations (vertical drift over Tirunelveli and ΔEEJ over Jicamarca) over the two antipodal locations is predominantly opposite during this interval (Figure 3c).

Interval-V: IMF Bz turns northward in the interval-V (∼1710-1810 UT) and vertical drift becomes less downward indicating a eastward electric field perturbation at this time. This appears to be under the influence of overshielding electric field. After the overshielding electric field perturbation, the vertical drift values reach the quiet time levels.

Figure 4 is used to identify the presence of substorm activity, if any, during 1200-1900 UT that encompasses the intervals (I-VI) under consideration (Figure 3) on 24 December 2014. In this plot, the variations in the electron and ion fluxes measured from geosynchronous orbit are presented in subplots a-f and subplots g-l respectively. The LANL geosynchronous satellites are LANL-01A, LANL-02A, LANL-04A, LANL-97A, LANL-080, and LANL-084. Six energy bins for electrons and four energy bins for protons are used in this study. The electron energy bins are 50-75 keV, 75-105 keV, 105-150 keV, 150-225 keV, 228-315 keV and 315-500 keV whereas the ion energy bins are 0-75 keV, 75-113 keV, 113-170 keV, and 170-250 keV. Differently colored lines are used to represent the different energy channels. In addition, the electron flux variations at four energy channels (75 keV, 150 keV, 275 keV and 475 keV) from GOES-13 satellites are also shown in Figure 4m. Here also different colors corresponds to different energy channels. Two intervals are marked with gray (∼1406-1530 UT) and brown (∼1610-1700 UT) rectangular boxes in all the subplots of Figure 4. These are the same intervals that are marked for AE and PC indices in Figure 4e. There are weak substorm injection activities noticed during intervals 1410-1530 UT (particularly in LANL-01A) and 1610-1700 UT (particularly in LANL-04A). The first substorm onset happens around 1410 UT. At this time, LANL-01A detects identifiable ion injections. GOES-13 also sees dispersed electron injections ∼1410 UT. It is to be noted that both satellites are far (LANL-01A at 165°W and GOES-13 at 75°W) from the Indian sector. On the other hand, injection activities (with dispersion) are noticed in the electron as well as ion channels starting at ∼1630 UT which is particularly captured by LANL-04A (∼ 65°E). At this time, the injection activities are not captured by GOES- 13. This suggests energetic particle injection at the geosynchronous orbit closer to the location of LANL-04A. The other LANL satellites seem to be away from the proton injection front and as a consequence, the injection signatures are quite dispersed at the other satellite locations. Based on this figure, it appears that substorm is present during 1610-1700 UT closer to the Indian longitude. The implications of these results will be discussed in the discussion section.

Figure 5 depicts the variations in the north-south (X) component of the magnetic field along the Indian and the Peruvian (antipodal location of Indian longitude) longitudes starting from the northern high latitudes to the equatorial regions. ΔX variations of Indian and Peruvian magnetometer stations are shown with red/green and blue colored lines, respectively, in Figure 5a-d. Figure 5e shows the variations in IMF By and IMF Bz with blue and black colored lines, respectively (reproduced from Figure 1). The interval (∼1420-1530 UT, interval-II)is marked in this figure with green colored rectangular box. It can be noted that the ΔX variations are anti-correlated in Figure 5a and 5b (mid latitudes) and start becoming less anti-correlated and more correlated as one comes toward the low-equatorial latitudes (Figures 5c and 5d). As revealed by Figure 5e and also pointed out earlier, two positive peaks in IMF By with a negative excursion in between are observed in this interval. In addition, it is also shown in Figure 3c that ΔVd over Tirunelveli and ΔEEJ over Jicamarca are both positive during this time.

In order to evaluate the effects of disturbance dynamo during intervals I-V, Figure 6 is presented. Figures 6a-6f depict the latitudinal variations in D_{dyn} over the Jicamarca sector during 1300- 1845 UT in steps of 15 mins intervals. The values of D_{dyn} over the dip equatorial region is negative/nearly zero on all the times except during 1530-1545 UT (Figure 6c) and at 1800 UT (Figure 6f). Therefore, Figures 6c and 6f suggest small contributions of D_{dyn} during interval-III and -V respectively.

4 Discussion

The important role of prompt penetration electric field (PPEF) in enhancing zonal electric field during local PRE hours is evident on 24 December 2014 (see Figure 2a). This enhanced zonal electric field not only shifted the EIA crest but also caused enhancement in TEC over the crest region. Kumar et al. (2021, 2022) brought out the important role of PRE and solar flux dependence of the post-sunset enhancement of OI 630.0 nm airglow intensity and VTEC over the EIA crest region. Therefore, it is not surprising that an enhanced PRE (interval-I in Figure 3d) would enhance the VTEC as well as OI 630.0 nm airglow intensity over the EIA crest region as brought out in Figure 2b and 2c. However, what is different here is the sustained (till 2100 LT or 1600 UT) enhancement of VTEC (Figure 2b) and airglow intensity (Figure 2c) over the crest region and also the longer sustenance of the EIA crest location at a higher latitude of 12.5° (Figure 2d) on the event day. It is also important to note that strength of EEJ_{India} on 24 December, 2014 is, in fact, weaker compared to the other days. Despite that, we see an elevated OI 630.0 nm airglow intensity over the EIA crest region on this night. Therefore, it is apparent that the enhancements in VTEC and 630.0 nm airglow intensity on this night are not due to conditioning of the EIA crest region by the daytime F region plasma fountain process driven by daytime zonal electric field over the equatorial ionosphere. Elevated $h'F$ over Tirunelveli in the evening hours of 24 December, 2014 provides the first clue that the impact on the EIA crest region on this night is because of what happened in the evening hours. It is noteworthy that the EIA crest is located at 12.5°N magnetic latitude till 2015 LT on the quiet day as indicated in Figure 2d. The fact that the vertical drift does not really become downward on the event day during the post-sunset hours (Figure 2a) and also get significantly upward at $\sim$ 1600 UT (2100 LT) have important connection with the behavior of EIA crest on the event night. This essentially means that the electric field is eastward at 2100 LT on this night. This is in contrast with the results of Liu et al. (2013) and Le et al. (2014) who showed the primary role of westward electric field in the pre-midnight hours in the enhancements of ionospheric plasma density over low latitudes. It is to be noted that under geomagnetically quiet conditions, westward electric field is expected during 2100-2200 LT and the mechanisms suggested by Liu et al. (2013) and Le et al. (2014) are important. However, as pointed out earlier, the plasma density enhancement in the present case is connected with the eastward electric field polarity over low latitudes. Therefore, the processes responsible for the unusual behavior of the vertical drift (proxy for the zonal electric field) on this night deserve critical attention. Once we understand the possible causative mechanisms for this eastward electric field perturbation, we will come back to the topic of plasma density enhancement at this local time.

To understand the anomalous behavior of the zonal electric field on 24 December, 2014, we now shift our attention to intervals II-IV in Figure 3. Note, IMF Bz is southward in these intervals. However, IMF Bz is more southward (IEFy is more positive) during intervals-II and -IV compared to interval-III. In view of this, we expect more changes in the equatorial vertical drift during intervals II and IV compared to interval-III. However, what we observe is contrary to this expectation and hence counter-intuitive. The perturbations in the electric field is nominally eastward (nominally upward drift or nearly zero drift) which is followed by an increase in eastward perturbation in the interval-II and significantly westward perturbation in the interval-IV. On the contrary, in the interval-III, the eastward electric field perturbations keeps increasing. Another interesting feature is the observation that vertical drift keeps increasing through intervals II and III although IMF Bz becomes less southward in interval-III compared to interval-II. Therefore, even if eastward penetration electric field is operational during this period that resists the drifts to turn downward, one expects larger drifts when IMF Bz (or IEFy) is larger. This suggests contribution from other driver(s). Therefore, not only these observations cannot be explained by the eastward penetration electric field perturbations expected till 2200 LT as per the existing understanding (e.g., Fejer et al., 2008b; Nopper Jr.

& Carovillano, 1978) but the amplitude of perturbations also need attention here. Importantly, LANL geosynchronous particle fluxes (Figure 4) confirm that there is no significant substorm occurrence closer to Indian longitude during the interval of first enhancements of AE and PC indices that occur during interval-II. Further, the interval of the first and strong enhancements in AE and PC indices are also marked by relatively large magnitude of IEFy. This suggests strong influence of IEFy in the enhancements of AE and PC indices at this time. This leads us to envisage a strong IMF By role in the interval-II. From the work of Chakrabarty et al. (2017), we know that predominantly positive IMF By can rotate the DP2 convection cells (well-developed during southward IMF Bz condition) significantly so that the daytime eastward pertubation electric field encroach into the post-sunset sector and affects the polarity of the perturbation electric field during post-sunset hours. This gets credence from the present observations (Figure 3c) wherein the polarity of ΔEEJ and vertical drift over the Jicamarca and Indian sectors are identical during interval-II suggesting an eastward electric field perturbations over both the sectors (Jicamarca is the day sector whereas Tirunelveli is in the night sector). Note, this is the local time over the Indian sector when an westward electric field polarity (downward drift as per quiet day pattern) is expected. Considering the curl-free nature of the ionospheric electric field and maximum impact of the penetration electric field on the ionospheric zonal component, one may expect opposite polarities of perturbation electric field at the day and night side of the dip equatorial ionosphere. This is evident in earlier results also (e,g., see Figure 3 of Kelley & Makela, 2002). Therefore, it appears that the identical polarity of penetration electric field over both Indian and Jicamarca sectors during interval-II are possibly due to the effects of IMF By. Although based on these low cadence observations of drifts, it is difficult to evaluate the relative roles of magnitude and polarity reversal of IMF By, supporting evidences in the form of identical polarity of electric field perturbations over antipodal locations and specific pattern (discussed subsequently) of global ΔX variations reinforce the role of IMF By. The proposition of the rotation of the DP2 convection cells by the effects of IMF By (e.g., Chakrabarty et al., 2017) gets further credence from Figure 5 wherein one can see the anti-correlation of ΔX variations over mid latitudes but correlation over low latitudes. Kelley and Makela (2002) found the westward penetration of electric field over Jicamarca during the pre-midnight hours under the southward IMF Bz conditions and suspected the effect of IMF By. In the work of Chakrabarty et al. (2017) and this work, we see the IMF By effect during the post-sunset hours. This is consistent with the work of Hui and Vichare (2021) who, using TIE-GCM simulations, showed that the effects of IMF By over low latitudes are most prominent at the terminator sector over low latitudes.

At this juncture, we note that ΔEEJ and ΔVd (Figure 3c) show anti-correlations during intervals-III and IV which is consistent with the curl-free nature of the ionospheric electric field as discussed in the previous paragraph. However, zonal electric field perturbations over the Indian sector is eastward and westward respectively during these intervals. Unlike interval-II, ΔX variations (Figure 5) during these intervals do not show any systematic changes in the behavior as one comes towards the low latitude (mentioned in the previous paragraph) and this is indicative of the absence of IMF By effect during intervals -III and IV. Therefore, although IMF By turns positive during interval-III, we rule out IMF By effect during this interval and it get credence form Figure 5 too. This also indicates that the changes in IMF By is a necessary but not sufficient condition for it's effects to be detected in the electric field perturbations over the dip equator. This may be essentially due to the fact that the combined effects of IMF Bz and IMF By may not bring two antipodal stations under the same DP2 cell. We feel that the local time dependence of IMF By effects needs attention in the future.

Let us now investigate interval-III. In absence of any substorm onset activity during interval-III, the only way an enhanced eastward electric field perturbation can arise with a reduced (compared to interval-II) amplitude of southward IMF Bz condition is through the withdrawal of IMF By effect that was present before. In addition, during interval-III, some effects of eastward DD electric field perturbations cannot be ruled out as suggested by Figure 6c. However, it is not clear why DD effects that can last for a much longer duration (e.g., Fejer et al., 2017; Zhang et al., 2017, 2019) turns effective only for a short duration. Fejer et al. (2008b) shows that the polarity of DD electric field perturbation is eastward only after 2100 LT and it is westward during 1700-2100 LT (as is the case here). This also suggests that any eastward electric field perturbation during 1700-2100 LT might not be affected by DD effects significantly. We, therfore, suggest that the usual eastward penetration electric field perturbations are experienced over the Indian sector during interval-II under the influence of southward IMF Bz (dawn-to-dusk IEFy) with no modification offered by IMF By and possibly some contribution of DD electric field. As a consequence, the eastward electric field perturbation seems to increase at this time. On the other hand, during interval-IV, we notice westward penetration electric field that causes downward drift. There is no influence of disturbance dynamo observed during this interval (Figure 6). We propose that the penetration electric field is already westward during this time on this night which is, in general, expected at $\sim$ 2200 LT as some of the earlier works (e.g., Fejer et al., 2008b) suggested. However, the magnitude of the westward electric field perturbations during interval-IV cannot be explained by the IEFy magnitude during this time with even 10-15% penetration efficiency and 10% uncertainty in the drift magnitude. Although the AE and PC indices show minor enhancements during interval IV, LANL-04A observations suggest the presence of substorm related particle injections at the geosynchronous orbit closer to the Indian longitude (Figure 4). On the other hand, IEFy starts decreasing during this interval. Therefore, we suggest that the combined effects of penetration electric fields due to IEFy and substorm cause the unusually large westward electric field perturbation during interval-IV. Earlier works by Hui et al. (2017) and Rout et al. (2019) show that substorm induced electric field can enhance the conventional penetration electric fields in a significant manner. However, it is to be kept in mind, that substorms have been shown earlier to cause both eastward (e.g., Chakrabarty et al., 2008, 2010; Huang, 2009; Hui et al., 2017; Rout et al., 2019) and westward (e.g., Kikuchi et al., 2000; Chakrabarty et al., 2015; Hui et al., 2017) electric field perturbations over the equatorial ionosphere.

During the interval-V ($\sim$2210-2310 LT, see Figure 3d), the IMF Bz turns northward from southward, and an overshielding electric field (e.g., Kelley et al., 1979; Gonzales et al., 1979; Fejer et al., 1979) is imposed over the equatorial ionosphere. This provides the eastward perturbations to the ionospheric electric field. In addition, a small effect of DD electric field may be presented at 2300 LT (1800 UT) as suggested by Figure 6f. Owing to this, vertical drift becomes less downward during the interval-V. It has been shown earlier (e.g., Chakrabarty et al., 2006; Sekar & Chakrabarty, 2008; Rout et al., 2019) that on many occasions, the nighttime eastward electric field perturbations due to overshieding effect can affect the equatorial F region vertical drifts significantly.

Last but not the least, two peaks are observed in VTEC (Figure 2b) and 630.0 nm airglow intensity (Figure 2c) during the post-sunset hours on 24 December 2014. The peaks are more conspicuous in the airglow intensity variation. The first peak occurs at $\sim$ 1445 UT (1945 LT) that is separated from the peak PRE drift (occurs at $\sim$ 13 UT or 18 LT) by around 1.75 hrs. This is consistent with the results of Kumar et al. (2021). The second peak that occurs just before 1600 UT (or 2100 LT) is probably a consequence of less quenching as the ionosphere goes up in altitude simultaneously over the entire low latitude due to the imposition of eastward penetration electric field.

5 Role of IMF By: Unresolved issues

Identification of the role of IMF By on equatorial ionosphere is a complex problem as we feel that southward IMF Bz is pre-condition on which the effects of IMF By should operate. This inference is true for high latitude. For equatorial latitudes, there are two aspects that are not clear at the present moment. First, what are the optimal magnitudes of southward IMF Bz and IMF By under which the IMF By effects will be discernible? Although, some studies in this regard have been carried out for high latitudes (e.g., Ruohoniemi & Greenwald, 2005), this has not been studied over dip equatorial region. Second, whether IMF By magnitude is more important or polarity reversal in IMF By is more important? Based on the present study and the earlier work (Chakrabarty et al., 2017), we can speculate that both factors can be important and what matters is the combined effects of the resizing of DP2 cells by the southward IMF Bz, rotation of the cells by IMF By, the relative position of the station where IMF By effects are to be detected and finally, the local time at which it is to be detected. It is also clear that one needs high temporal resolution vertical drift data to capture the effects of the sharp changes in IMF By under southward IMF Bz condition. Note, over the Indian sector, there is no incohorent scatter radar and the vertical drifts during nighttime over the dip equatorial region can only be derived based on ionospheric height variations with temporal resolution of 10 mins or 15 mins under normal circumstances. This is why we abstain from evaluating the relative roles of magnitude and polarity reversal of IMF By based on the present drift datasets the cadence of which is 10 mins.

In order to garner further evidence on the importance of high cadence data, we compare one minute cadence data of ΔX over Huancayo (in blue) with IMF By (in red) and IMF Bz (in magenta) separately in Figure 7. The intervals II (in green) and III (in orange) in Figure 7 are marked in the same way as that in Figure 3. It is to be noted that Huancayo is in day sector during intervals II and III. Therefore, if we consider that daytime ionospheric conductivity does not change significantly (which is a reasonable assumption) during intervals II and III ($\sim$2 hrs), the changes in ΔX can be attributed to ionospheric electric field variations. It is interesting to note that the variations in ΔX over Huancayo and IMF By go hand in hand in interval II and a phase offset starts coming up in interval III. During interval III, IMF Bz does not change much but IMF By changes significantly although with a phase delay. Therefore, it is possible that the influence of IMF By weakens during interval III. Since the cadence of ΔX variations is one minute, this provides credence to the proposition of the influence of IMF By during interval II. Eventually, the yardstick that we follow (and highlighted in Chakrabarty et al., 2017) for the detection of IMF By effect (under southward IMF Bz) is the identical polarity of electric field perturbations over antipodal stations (Figure 3c) and the systematic variations in ΔX from high to low latitudes as shown in Figure 5.

6 Conclusions

The space weather event on 24 December 2014 reported provides a number of critical insights on the nature of the penetration electric field. First, the equatorial/low latitude impact is anomalously enhanced during the post-sunset hours of 24 December 2014 when the magnitude of IEFy is not very large but persists through local PRE/post-PRE hours. This suggest that as far as the low latitude ionospheric impacts are considered, the local time of the electric field disturbance is important. Penetration electric field perturbations occurring during PRE hours when the zonal electric field is already enhanced can make the equatorial impact unusually stronger. Second, during one single event, we see occasion when a number of phenomenologically different penetration electic fields (like penetration electric fields due to IEFy, substorm and disturbance dynamo etc.) acting simultaneously on the equatorial ionosphere. Therefore, the magnitude of electric field perturbations on some occasions cannot be determined based on the existing paradigm of penetration electric fields. Third and most importantly, due to the additional effects of IMF By for some time, the response of the equatorial electric field perturbations turns out to be anomalous both in terms of magnitude and polarity. These anomalous effects need more attention in future for a comprehensive phenomenological understanding of the nature of the penetration electric fields.

Acknowledgments

Ap and Sym-H indices are taken from the World Data Center for Geomagnetism, Kyoto (http://wdc.kugi.kyoto-u.ac.jp/). Solar wind parameters are obtained from NASA GSFC CDAWeb (http://cdaweb.gsfc.nasa.gov/). The magnetometer data along the Jicamarca and Indian longitudes are obtained from SuperMag (https://supermag.jhuapl.edu/). 1 minute corrected data over Jicamarca and Leticia are taken from the Low Latitude Ionospheric Sensor Network (LISN) (http://lisn.igp.gob.pe/). We acknowledge the work of all the PIs and support staff for whom these data could be made available. D. Rout acknowledges the support from Humboldt Research Fellowship for Postdoctoral Researchers (Humboldt foundation grants PSP D-023-20- 001). The remaining datasets can be obtained from `http://dx.doi.org/10.17632/xhm84smdvb.1`. This work is supported by the Department of Space, Government of India.

References

Abdu, M. A., Nogueira, P. A. B., Santos, A. M., de Souza, J. R., Batista, I. S., & Sobral, J. H. A. (2018). Impact of disturbance electric fields in the evening on prereversal vertical drift and spread f developments in the equatorial ionosphere. *Annales Geophysicae*, *36*(2), 609–620. Retrieved from `https://angeo.copernicus.org/articles/36/609/2018/` doi: 10.5194/angeo-36-609-2018

Amory-Mazaudier, C., Bolaji, O. S., & Doumbia, V. (2017). On the historical origins of the cej, dp2, and ddyn current systems and their roles in the predictions of ionospheric responses to geomagnetic storms at equatorial latitudes. *Journal of Geophysical Research: Space Physics*, *122*(7), 7827-7833. doi: https://doi.org/10.1002/2017JA024132

Anderson, D., & Rusch, D. (1980). Composition of the nighttime ionospheric f 1 region near the magnetic equator. *Journal of Geophysical Research: Space Physics*, *85*(A2), 569-574. doi: https://doi.org/10.1029/JA085iA02p00569

Angelopoulos, V., Coroniti, F. V., Kennel, C. F., Kivelson, M. G., Walker, R. J., Russell, C. T., . . . Harris, T. (1996). Multipoint analysis of a bursty bulk flow event on april 11, 1985. *Journal of Geophysical Research: Space Physics*, *101*(A3), 4967-4989. doi: https://doi.org/10.1029/95JA02722

Baker, D. N., Pulkkinen, T. I., Hesse, M., & McPherron, R. L. (1997). A quantitative assessment of energy storage and release in the earth's magnetotail. *Journal of Geophysical Research: Space Physics*, *102*(A4), 7159-7168. doi: https://doi.org/10.1029/96JA03961

Balan, N., Liu, L., & Le, H. (2018). A brief review of equatorial ionization anomaly and ionospheric irregularities. *Earth and Planetary Physics*, *2*(4), 257-275. doi: 10.26464/epp2018025

Balan, N., Shiokawa, K., Otsuka, Y., Watanabe, S., & Bailey, G. J. (2009). Super plasma fountain and equatorial ionization anomaly during penetration electric field. *Journal of Geophysical Research: Space Physics*, *114*(A3). doi: https://doi.org/10.1029/2008JA013768

Bittencourt, J. A., & Abdu, M. A. (1981). A theoretical comparison between apparent and real vertical ionization drift velocities in the equatorial f region. *Journal of Geophysical Research: Space Physics*, *86*(A4), 2451-2454. doi: 10.1029/JA086iA04p02451

Blanc, M., & Richmond, A. (1980). The ionospheric disturbance dynamo. *Journal of Geophysical Research: Space Physics*, *85*(A4), 1669-1686. doi: https://doi.org/10.1029/JA085iA04p01669

Chakrabarty, D., Hui, D., Rout, D., Sekar, R., Bhattacharyya, A., Reeves, G. D., & Ruohoniemi, J. M. (2017). Role of imf by in the prompt electric field disturbances over equatorial ionosphere during a space weather event. *Journal of Geophysical Research: Space Physics*, *122*(2), 2574-2588. doi:

https://doi.org/10.1002/2016JA022781

Chakrabarty, D., Rout, D., Sekar, R., Narayanan, R., Reeves, G. D., Pant, T. K., ... Shiokawa, K. (2015). Three different types of electric field disturbances affecting equatorial ionosphere during a long-duration prompt penetration event. *Journal of Geophysical Research: Space Physics*, *120*(6), 4993-5008. doi: 10.1002/2014JA020759

Chakrabarty, D., Sekar, R., Narayanan, R., Devasia, C. V., & Pathan, B. M. (2005). Evidence for the interplanetary electric field effect on the oi 630.0 nm airglow over low latitude. *Journal of Geophysical Research: Space Physics*, *110*(A11). doi: https://doi.org/10.1029/2005JA011221

Chakrabarty, D., Sekar, R., Narayanan, R., Patra, A. K., & Devasia, C. V. (2006). Effects of interplanetary electric field on the development of an equatorial spread f event. *Journal of Geophysical Research: Space Physics*, *111*(A12). doi: https://doi.org/10.1029/2006JA011884

Chakrabarty, D., Sekar, R., Sastri, J. H., Pathan, B. M., Reeves, G. D., Yumoto, K., & Kikuchi, T. (2010). Evidence for oi 630.0 nm dayglow variations over low latitudes during onset of a substorm. *Journal of Geophysical Research: Space Physics*, *115*(A10). doi: https://doi.org/10.1029/2010JA015643

Chakrabarty, D., Sekar, R., Sastri, J. H., & Ravindran, S. (2008). Distinctive effects of interplanetary electric field and substorm on nighttime equatorial f layer: A case study. *Geophysical Research Letters*, *35*(19). doi: 10.1029/2008GL035415

Emmert, J. T., Drob, D. P., Picone, J. M., Siskind, D. E., Jones Jr., M., Mlynczak, M. G., ... Yuan, T. (2021). Nrlmsis 2.0: A whole-atmosphere empirical model of temperature and neutral species densities. *Earth and Space Science*, *8*(3), e2020EA001321. doi: https://doi.org/10.1029/2020EA001321

Fejer, B. G., Blanc, M., & Richmond, A. D. (2017). Post-storm middle and low-latitude ionospheric electric fields effects. *Space Science Reviews*, *206*(1), 407–429. doi: https://doi.org/10.1007/s11214-016-0320-x

Fejer, B. G., Gonzales, C., Farley, D., Kelley, M., & Woodman, R. (1979). Equatorial electric fields during magnetically disturbed conditions 1. the effect of the interplanetary magnetic field. *Journal of Geophysical Research: Space Physics*, *84*(A10), 5797-5802. doi: https://doi.org/10.1029/JA084iA10p05797

Fejer, B. G., Jensen, J. W., & Su, S.-Y. (2008a). Quiet time equatorial F region vertical plasma drift model derived from ROCSAT-1 observations. *Journal of Geophysical Research: Space Physics*, *113*(A5). doi: 10.1029/2007JA012801

Fejer, B. G., Jensen, J. W., & Su, S.-Y. (2008b). Seasonal and longitudinal dependence of equatorial disturbance vertical plasma drifts. *Geophysical Research Letters*, *35*(20). doi: https://doi.org/10.1029/2008GL035584

Fejer, B. G., Navarro, L. A., Sazykin, S., Newheart, A., Milla, M. A., & Condor, P. (2021). Prompt penetration and substorm effects over jicamarca during the september 2017 geomagnetic storm. *Journal of Geophysical Research: Space Physics*, *126*(8), e2021JA029651. doi: https://doi.org/10.1029/2021JA029651

Gonzales, C., Kelley, M., Fejer, B., Vickrey, J., & Woodman, R. (1979). Equatorial electric fields during magnetically disturbed conditions 2. implications of simultaneous auroral and equatorial measurements. *Journal of Geophysical Research: Space Physics*, *84*(A10), 5803-5812. doi: https://doi.org/10.1029/JA084iA10p05803

Hashimoto, K. K., Kikuchi, T., Tomizawa, I., & Nagatsuma, T. (2017). Substorm overshielding electric field at low latitude on the nightside as observed by the hf doppler sounder and magnetometers. *Journal of Geophysical Research: Space Physics*, *122*(10), 10,851-10,863. doi: https://doi.org/10.1002/2017JA024329

Henderson, M. G., Reeves, G. D., Belian, R. D., & Murphree, J. S. (1996). Observations of magnetospheric substorms occurring with no apparent solar wind/imf trigger. *Journal of Geophysical Research: Space Physics*, *101*(A5), 10773-10791. doi: https://doi.org/10.1029/96JA00186

Huang, C.-S. (2009). Eastward electric field enhancement and geomagnetic positive bay in the dayside low-latitude ionosphere caused by magnetospheric substorms during sawtooth events. *Geophysical Research Letters*, *36*(18). doi: https://doi.org/10.1029/2009GL040287

Huang, C.-S., Foster, J. C., Goncharenko, L. P., Reeves, G. D., Chau, J. L., Yumoto, K., & Kitamura, K. (2004). Variations of low-latitude geomagnetic fields and dst index caused by magnetospheric substorms. *Journal of Geophysical Research: Space Physics*, *109*(A5). doi: https://doi.org/10.1029/2003JA010334

Huang, C.-S., Sazykin, S., Chau, J. L., Maruyama, N., & Kelley, M. C. (2007). Penetration electric fields: Efficiency and characteristic time scale. *Journal of Atmospheric and Solar-Terrestrial Physics*, *69*(10), 1135-1146. doi: https://doi.org/10.1016/j.jastp.2006.08.016

Huang, C.-S., Yumoto, K., Abe, S., & Sofko, G. (2008). Low-latitude ionospheric electric and magnetic field disturbances in response to solar wind pressure enhancements. *Journal of Geophysical Research: Space Physics*, *113*(A8). doi: https://doi.org/10.1029/2007JA012940

Hui, D., Chakrabarty, D., Sekar, R., Reeves, G. D., Yoshikawa, A., & Shiokawa, K. (2017). Contribution of storm time substorms to the prompt electric field disturbances in the equatorial ionosphere. *Journal of Geophysical Research: Space Physics*, *122*(5), 5568-5578. doi: https://doi.org/10.1002/2016JA023754

Hui, D., & Vichare, G. (2021). Influence of imf-by on the equatorial ionospheric plasma drifts: Tiegcm simulations. *Journal of Geophysical Research: Space Physics*, *126*(9), e2021JA029270. doi: https://doi.org/10.1029/2021JA029270

Kelley, M. C., Fejer, B. G., & Gonzales, C. A. (1979). An explanation for anomalous equatorial ionospheric electric fields associated with a northward turning of the interplanetary magnetic field. *Geophysical Research Letters*, *6*(4), 301-304. doi: https://doi.org/10.1029/GL006i004p00301

Kelley, M. C., & Makela, J. J. (2002). By-dependent prompt penetrating electric fields at the magnetic equator. *Geophysical Research Letters*, *29*(7), 57-1-57-3. doi: https://doi.org/10.1029/2001GL014468

Kelley, M. C., Makela, J. J., Chau, J. L., & Nicolls, M. J. (2003). Penetration of the solar wind electric field into the magnetosphere/ionosphere system. *Geophysical Research Letters*, *30*(4). doi: https://doi.org/10.1029/2002GL016321

Kikuchi, T., Hashimoto, K. K., Kitamura, T.-I., Tachihara, H., & Fejer, B. (2003). Equatorial counterelectrojets during substorms. *Journal of Geophysical Research: Space Physics*, *108*(A11). doi: https://doi.org/10.1029/2003JA009915

Kikuchi, T., Hashimoto, K. K., & Nozaki, K. (2008). Penetration of magnetospheric electric fields to the equator during a geomagnetic storm. *Journal of Geophysical Research: Space Physics*, *113*(A6). doi: https://doi.org/10.1029/2007JA012628

Kikuchi, T., Lühr, H., Schlegel, K., Tachihara, H., Shinohara, M., & Kitamura, T.-I. (2000). Penetration of auroral electric fields to the equator during a substorm. *Journal of Geophysical Research: Space Physics*, *105*(A10), 23251-23261. doi: https://doi.org/10.1029/2000JA900016

Klimas, A. J., Valdivia, J. A., Vassiliadis, D., Baker, D. N., Hesse, M., & Takalo, J. (2000). Self-organized criticality in the substorm phenomenon and its relation to localized reconnection in the magnetospheric plasma sheet. *Journal of Geophysical Research: Space Physics*, *105*(A8), 18765-18780. doi: https://doi.org/10.1029/1999JA000319

Kumar, A., Chakrabarty, D., Pandey, K., Fejer, B. G., Sunda, S., Seemala, G. K., ... Yadav, A. K. (2021). Evidence for the significant differences in response times of equatorial ionization anomaly crest corresponding to plasma fountains during daytime and post-sunset hours. *Journal of Geophysical Research: Space*

Physics, *126*(3), e2020JA028628. doi: https://doi.org/10.1029/2020JA028628
Kumar, A., Chakrabarty, D., Pandey, K., & Yadav, A. K. (2022). Solar flux dependence of post-sunset enhancement in vertical total electron content over the crest region of equatorial ionization anomaly. *Journal of Geophysical Research: Space Physics*, *127*(5), e2021JA030156. doi: https://doi.org/10.1029/2021JA030156
Le, H., Liu, L., Chen, Y., Zhang, H., & Wan, W. (2014). Modeling study of nighttime enhancements in f region electron density at low latitudes. *Journal of Geophysical Research: Space Physics*, *119*(8), 6648-6656. doi: https://doi.org/10.1002/2013JA019295
Liu, L., Chen, Y., Le, H., Ning, B., Wan, W., Liu, J., & Hu, L. (2013). A case study of postmidnight enhancement in f-layer electron density over sanya of china. *Journal of Geophysical Research: Space Physics*, *118*(7), 4640-4648. doi: https://doi.org/10.1002/jgra.50422
Lu, G., Goncharenko, L., Nicolls, M. J., Maute, A., Coster, A., & Paxton, L. J. (2012). Ionospheric and thermospheric variations associated with prompt penetration electric fields. *Journal of Geophysical Research: Space Physics*, *117*(A8). doi: https://doi.org/10.1029/2012JA017769
Lyons, L. R. (1995). A new theory for magnetospheric substorms. *Journal of Geophysical Research: Space Physics*, *100*(A10), 19069-19081. doi: https://doi.org/10.1029/95JA01344
Lyons, L. R. (1996). Substorms: Fundamental observational features, distinction from other disturbances, and external triggering. *Journal of Geophysical Research: Space Physics*, *101*(A6), 13011-13025. doi: https://doi.org/10.1029/95JA01987
Lyons, L. R., Blanchard, G. T., Samson, J. C., Lepping, R. P., Yamamoto, T., & Moretto, T. (1997). Coordinated observations demonstrating external substorm triggering. *Journal of Geophysical Research: Space Physics*, *102*(A12), 27039-27051. doi: https://doi.org/10.1029/97JA02639
MacDougall, J., Grant, I., & Shen, X. (1995). The canadian advanced digital ionosonde: design and results. *URSI INAG Ionospheric Station Inf. Bulletin, UAG-104*.
Manke, A. A., & Chakarabarty, D. (2016). An integrated software platform for gps/gnss ionospheric data analysis. *International Journal of Science, Engineering and Technology*, *4*(5). doi: 10.2348/ijset09160796
Mannucci, A. J., Tsurutani, B. T., Iijima, B. A., Komjathy, A., Saito, A., Gonzalez, W. D., … Skoug, R. (2005). Dayside global ionospheric response to the major interplanetary events of october 29–30, 2003 "halloween storms". *Geophysical Research Letters*, *32*(12). doi: https://doi.org/10.1029/2004GL021467
McPherron, R. L. (1979). Magnetospheric substorms. *Reviews of Geophysics*, *17*(4), 657-681. doi: https://doi.org/10.1029/RG017i004p00657
Nishida, A. (1968). Geomagnetic dp 2 fluctuations and associated magnetospheric phenomena. *Journal of Geophysical Research (1896-1977)*, *73*(5), 1795-1803. doi: https://doi.org/10.1029/JA073i005p01795
Nopper Jr., R. W., & Carovillano, R. L. (1978). Polar-equatorial coupling during magnetically active periods. *Geophysical Research Letters*, *5*(8), 699-702. doi: https://doi.org/10.1029/GL005i008p00699
Pandey, K., Chakrabarty, D., & Sekar, R. (2018). Critical evaluation of the impact of disturbance dynamo on equatorial ionosphere during daytime. *Journal of Geophysical Research: Space Physics*, *123*(11), 9762-9774. doi: https://doi.org/10.1029/2018JA025686
Rastogi, R., & Klobuchar, J. (1990). Ionospheric electron content within the equatorial f 2 layer anomaly belt. *Journal of Geophysical Research: Space Physics*, *95*(A11), 19045-19052. doi: https://doi.org/10.1029/JA095iA11p19045
Rastogi, R., & Patel, V. (1975). Effect of interplanetary magnetic field on ionosphere

over the magnetic equator. In *Proceedings of the indian academy of sciences-section a* (Vol. 82, pp. 121–141). doi: 10.1007/BF03046722

Reeves, G. D., McAdams, K. L., Friedel, R. H. W., & O'Brien, T. P. (2003). Acceleration and loss of relativistic electrons during geomagnetic storms. *Geophysical Research Letters*, *30*(10). doi: https://doi.org/10.1029/2002GL016513

Rout, D., Chakrabarty, D., Sekar, R., Reeves, G. D., Ruohoniemi, J. M., Pant, T. K., ... Shiokawa, K. (2016). An evidence for prompt electric field disturbance driven by changes in the solar wind density under northward imf bz condition. *Journal of Geophysical Research: Space Physics*, *121*(5), 4800-4810. doi: https://doi.org/10.1002/2016JA022475

Rout, D., Pandey, K., Chakrabarty, D., Sekar, R., & Lu, X. (2019). Significant electric field perturbations in low latitude ionosphere due to the passage of two consecutive icmes during 6–8 september 2017. *Journal of Geophysical Research: Space Physics*, *124*(11), 9494-9510. doi: 10.1029/2019JA027133

Ruohoniemi, J. M., & Greenwald, R. A. (2005). Dependencies of high-latitude plasma convection: Consideration of interplanetary magnetic field, seasonal, and universal time factors in statistical patterns. *Journal of Geophysical Research: Space Physics*, *110*(A9). doi: https://doi.org/10.1029/2004JA010815

Sastri, J. H., Rao, J. V. S. V., & Ramesh, K. B. (1993). Penetration of polar electric fields to the nightside dip equator at times of geomagnetic sudden commencements. *Journal of Geophysical Research: Space Physics*, *98*(A10), 17517-17523. doi: https://doi.org/10.1029/93JA00418

Savitzky, A., & Golay, M. J. (1964). Smoothing and differentiation of data by simplified least squares procedures. *Analytical chemistry*, *36*(8), 1627-1639.

Sekar, R., & Chakrabarty, D. (2008). Role of overshielding electric field on the development of pre-midnight plume event: Simulation results. *Journal of Atmospheric and Solar-Terrestrial Physics*, *70*(17), 2212-2221. doi: https://doi.org/10.1016/j.jastp.2008.04.015

Sekar, R., & Chakrabarty, D. (2011). A Review of the Recent Advances in the Investigation of Equatorial Spread F and Space Weather Effects over Indian Sector Using Optical and Other Techniques. In *Aeronomy of the earth's atmosphere and ionosphere* (p. 251-268). Springer.

Sripathi, S., Singh, R., Banola, S., Sreekumar, S., Emperumal, K., & Selvaraj, C. (2016). Characteristics of the equatorial plasma drifts as obtained by using canadian doppler ionosonde over southern tip of india. *Journal of Geophysical Research: Space Physics*, *121*(8), 8103-8120. doi: 10.1002/2016JA023088

Sunda, S., Sridharan, R., Vyas, B. M., Khekale, P. V., Parikh, K. S., Ganeshan, A. S., ... Bagiya, M. S. (2015). Satellite-based augmentation systems: A novel and cost-effective tool for ionospheric and space weather studies. *Space Weather*, *13*(1), 6-15. doi: 10.1002/2014SW001103

Tsurutani, B. T., Gonzalez, W. D., Guarnieri, F., Kamide, Y., Zhou, X., & Arballo, J. K. (2004). Are high-intensity long-duration continuous ae activity (hildcaa) events substorm expansion events? *Journal of Atmospheric and Solar-Terrestrial Physics*, *66*(2), 167-176. (Space Weather in the Declining Phase of the Solar Cycle) doi: https://doi.org/10.1016/j.jastp.2003.08.015

Tsurutani, B. T., Verkhoglyadova, O. P., Mannucci, A. J., Saito, A., Araki, T., Yumoto, K., ... Vasyliūnas, V. M. (2008). Prompt penetration electric fields (ppefs) and their ionospheric effects during the great magnetic storm of 30–31 october 2003. *Journal of Geophysical Research: Space Physics*, *113*(A5). doi: https://doi.org/10.1029/2007JA012879

Wang, H., Lühr, H., Zheng, Z., & Zhang, K. (2019). Dependence of the equatorial electrojet on auroral activity and in situ solar insulation. *Journal of Geophysical Research: Space Physics*, *124*(12), 10659-10673. doi: https://doi.org/10.1029/2019JA027320

Wang, W., Lei, J., Burns, A. G., Wiltberger, M., Richmond, A. D., Solomon,

S. C., ... Anderson, D. N. (2008). Ionospheric electric field variations during a geomagnetic storm simulated by a coupled magnetosphere ionosphere thermosphere (cmit) model. *Geophysical Research Letters*, *35*(18). doi: https://doi.org/10.1029/2008GL035155

Woodman, R. F., Chau, J. L., & Ilma, R. R. (2006). Comparison of ionosonde and incoherent scatter drift measurements at the magnetic equator. *Geophysical Research Letters*, *33*(1). doi: https://doi.org/10.1029/2005GL023692

Zaka, K. Z., Kobea, A. T., Assamoi, P., Obrou, O. K., Doumbia, V., Boka, K., ... Mene, N. M. (2009). Latitudinal profile of the ionospheric disturbance dynamo magnetic signature: comparison with the dp2 magnetic disturbance. *Annales Geophysicae*, *27*(9), 3523–3536. doi: 10.5194/angeo-27-3523-2009

Zhang, R., Liu, L., Le, H., & Chen, Y. (2019). Equatorial ionospheric electrodynamics over jicamarca during the 6–11 september 2017 space weather event. *Journal of Geophysical Research: Space Physics*, *124*(2), 1292-1306. doi: https://doi.org/10.1029/2018JA026295

Zhang, R., Liu, L., Le, H., Chen, Y., & Kuai, J. (2017). The storm time evolution of the ionospheric disturbance plasma drifts. *Journal of Geophysical Research: Space Physics*, *122*(11), 11,665-11,676. doi: https://doi.org/10.1002/2017JA024637

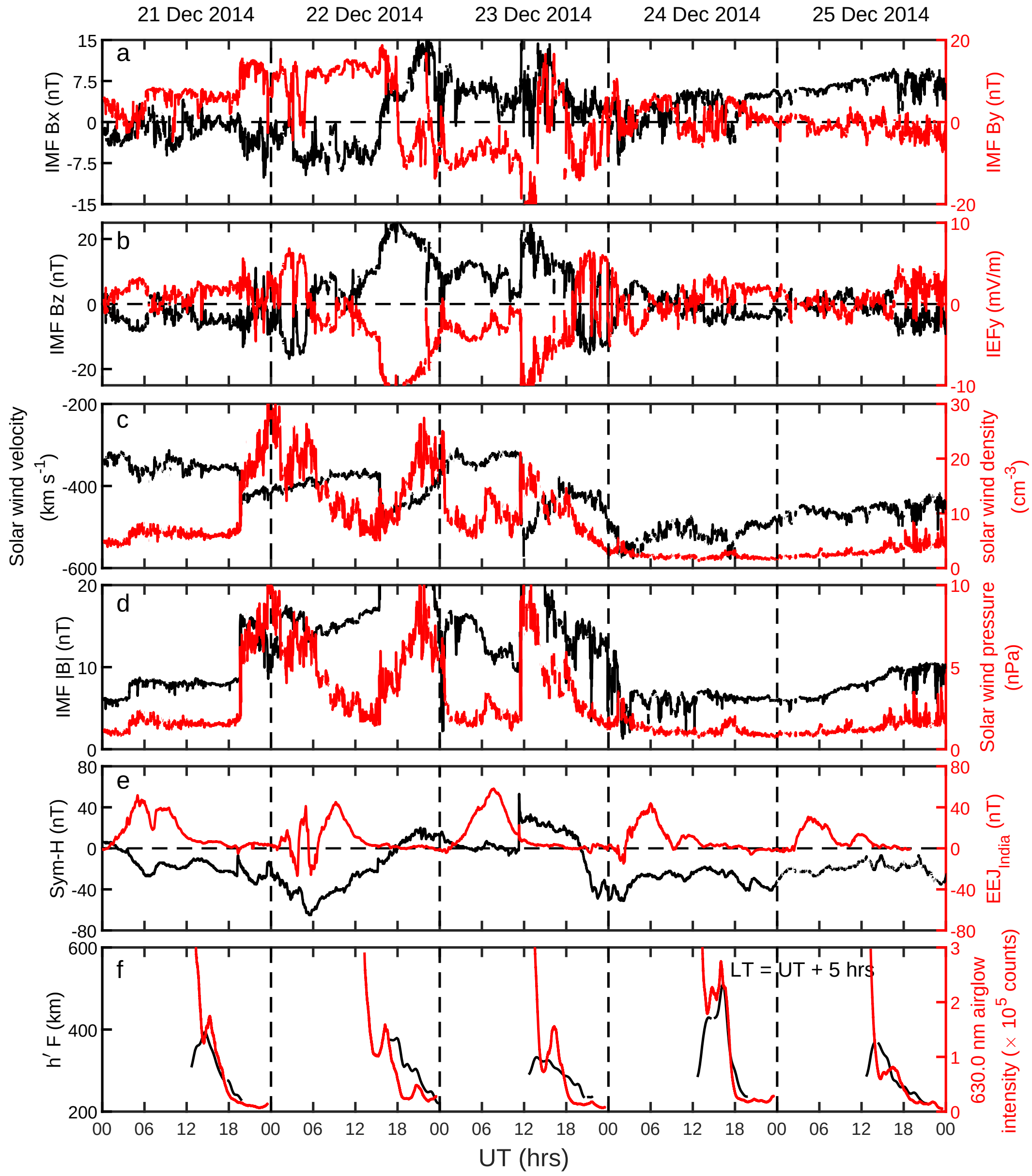

Figure 1. Variations in (a) IMF Bx (nT, black line) and IMF By (nT, red line), (b) IMF Bz (nT, black line) and IEFy (mV/m, red line), (c) solar wind velocity (kms^{-1}, black line) and density (cm^{-3}, red line), (d) IMF $|B|$ (nT, black) and pressure (nPa, red), (e) Sym-H index (nT, black) and equatorial electrojet strength (EEJ_{India}) over the Indian sector (nT, red), (f) $h'F$ (km, black) and OI 630.0 nm airglow intensity over Mt. Abu (in arbitrary units, red) from 21 December, 2014 to 25 December 2014.

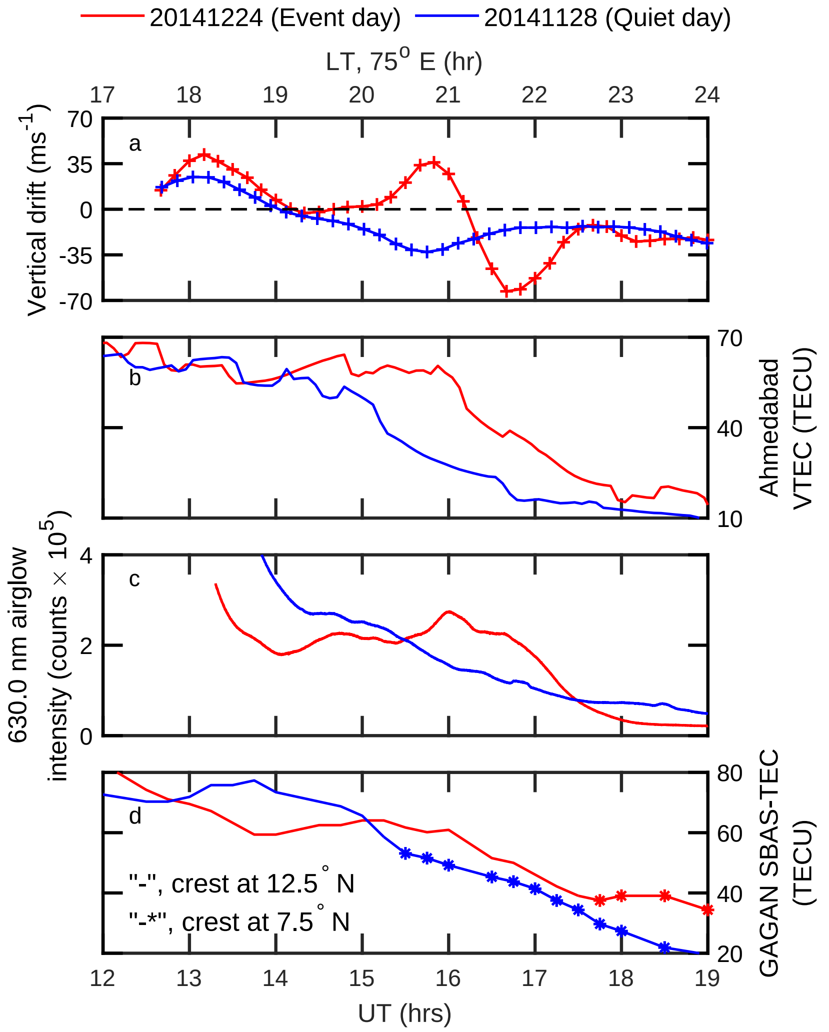

Figure 2. This figure illustrates the variations of a number of parameters on the event day (24 December 2014) and quiet day (28 November, 2014) with red and blue colors respectively. Subplots (a), (b), (c) and (d) represent vertical drifts (in ms^{-1}) over Tirunelveli, vertical total electron content (in TECU) over Ahmedabad, OI 630.0 nm airglow intensity (in arbiotrary unit) over Mt. Abu, and SBAS-TEC (in TECU) variations over only the crest location, respectively. In subplot (d), solid and solid lines with stars are used to show the position of the crest at 12.5° and 7.5° N magnetic latitudes.

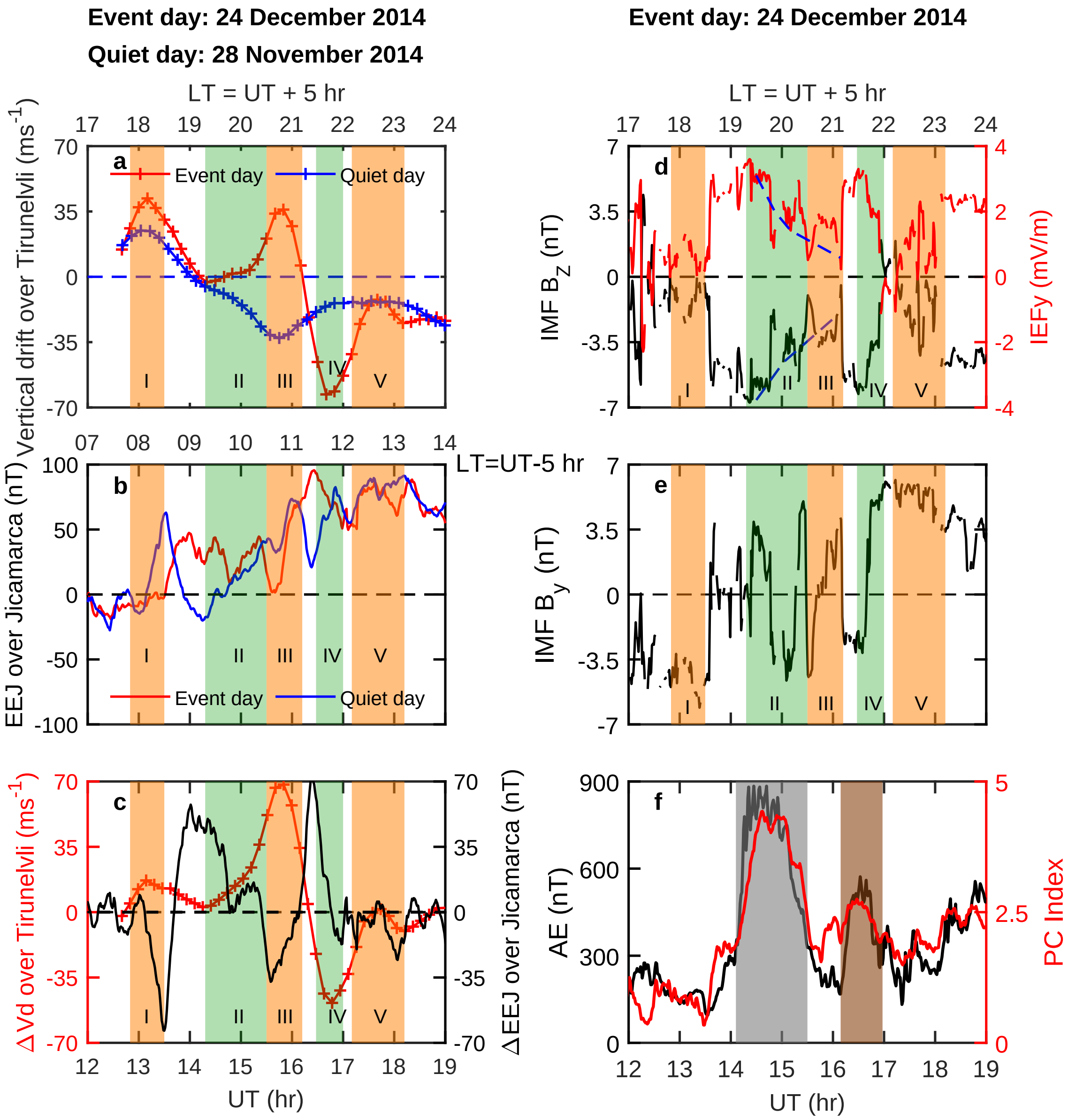

Figure 3. (a) shows the comparison of vertical drifts over Tirunelveli on the event day (24 December 2014, in red) with respect to a typical quiet day (28 November 2014, in blue) similar to what is shown in Figure 2a, (b) represents similar comparison in EEJ over Jicamarca, (c) shows the variations in the Δ Vd over Tirunelveli (in red) and ΔEEJ over Jicamarca (in black) obtained by subtracting the quiet day variation from the event day variation, (d) depicts the variations in IMF Bz (in black) and IEFy (in red), (e) represents the variations in IMF By and, (f) depicts the variations in the AE (in black) and PC (in red) indices. Based on vertical drift variations on event day, intervals (I-V) are marked with orange and green colored rectangular boxes in the panels (a-e). In (e), two conspicuous peaks in the AE and PC indices are marked with gray and brown colored rectangular boxes.

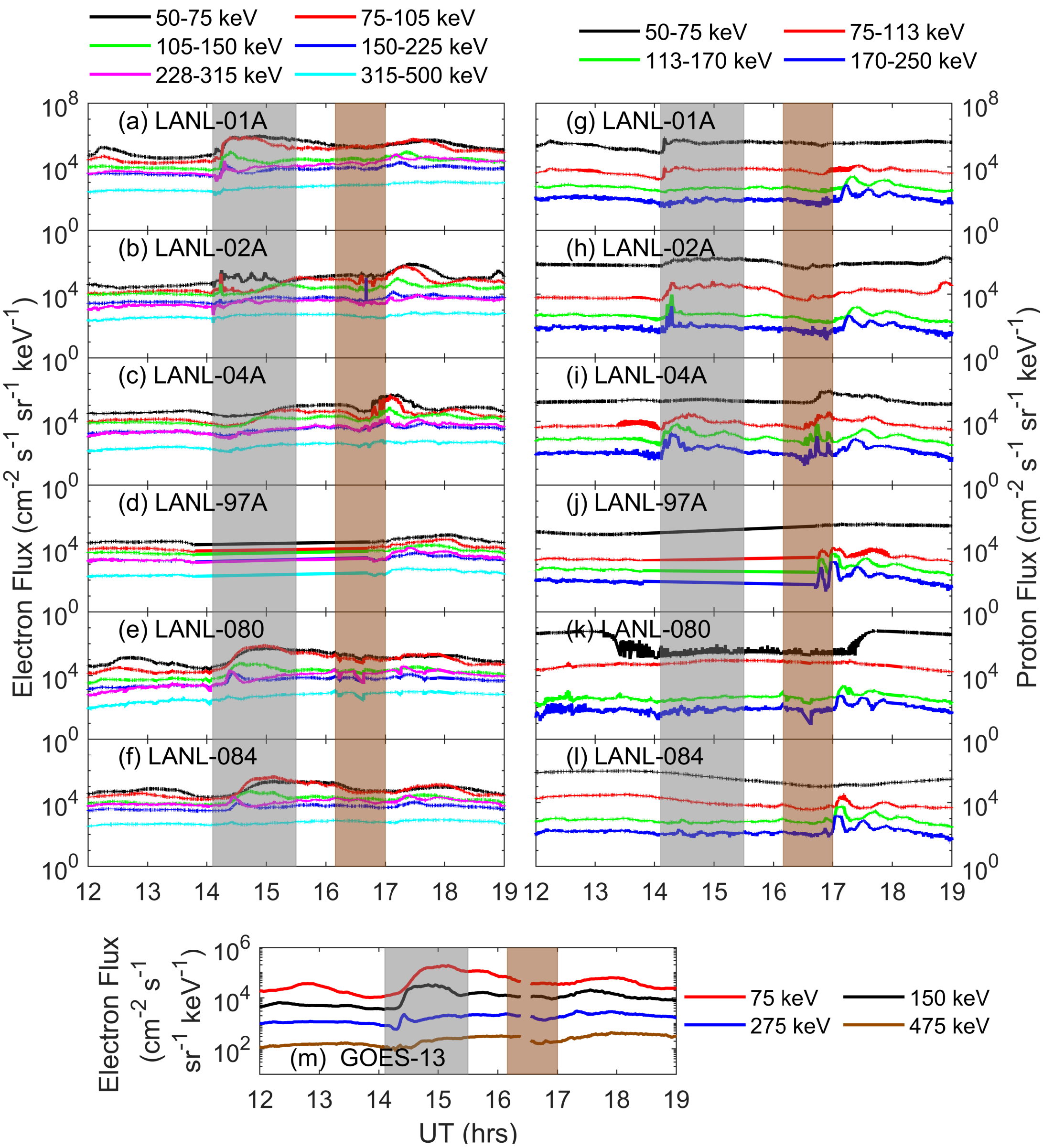

Figure 4. (a-f) and (g-l) represent the electron and proton flux variations measured by six LANL satellites (LANL-01A, LANL-02A, LANL-04A, LANL-97A, LANL-080, LANL-084) during 1200-1900 UT on 24 December 2014 for a number of energy channels mentioned at the top. (m) shows the electron flux variations at four energy channels (75 kev, 150 kev, 275 kev, 475 kev) measured by GOES-13 for same interval and day depicted in (a-l). Two intervals are marked with gray (∼1405-1530 UT) and brown (∼1610-1700 UT) rectangular boxes in all subplots, similarly marked in Figure 3f.

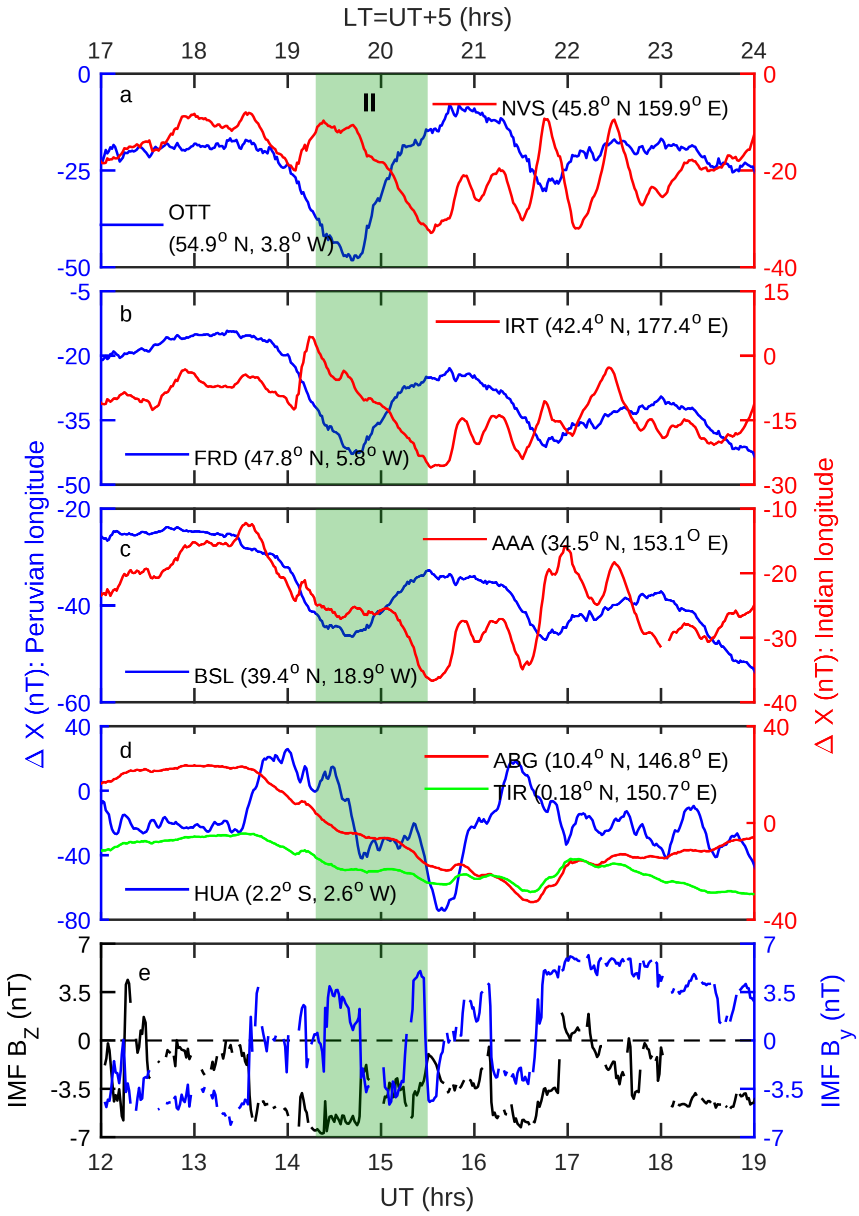

Figure 5. Variations of the northward component of magnetic field (ΔX) over Indian and Peruvian sectors from mid latitudes of the northern hemisphere to the equatorial region are shown in (a-d) with red/green and blue colors, respectively. (e) depicts the IMF Bz and IMF By in black and blue colors respectively. An interval is marked with green (∼1420-1530 UT) colored rectangular box when ΔX variations are anticorrelated over mid latitudes and start becoming correlated as one comes toward the low-equatorial latitudes.

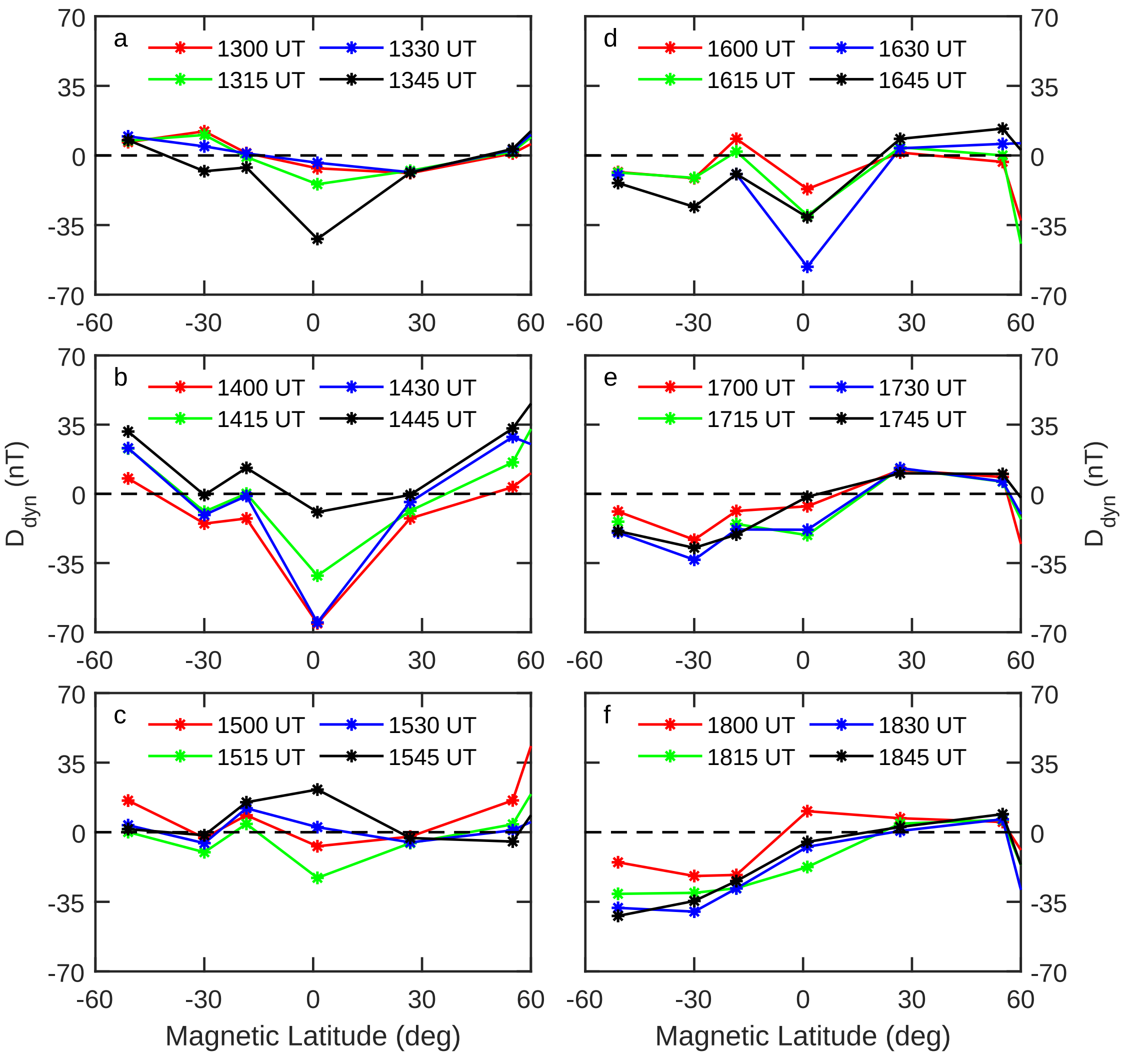

Figure 6. (a-f) show the latitudinal variations in D_{dyn} during 1300-1845 UT in steps of 15 mins intervals along Jicamarca longitudes on 24 December 2014. It can be seen that the positive deviations in D_{dyn} over equatorial latitudes are seen during 1530-1545 UT (in (c)) and 1800 UT (in (f)) indicating influence of disturbance dynamo effects.

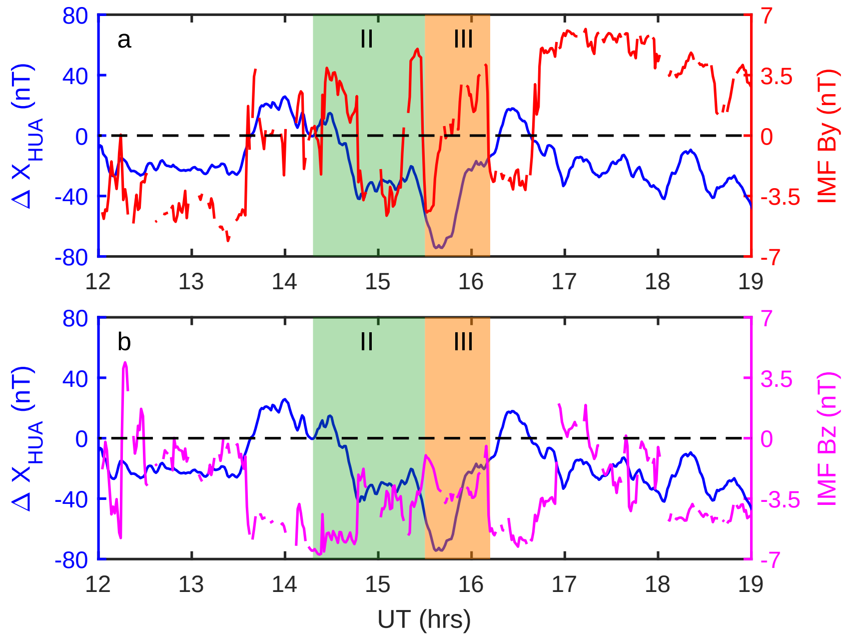

Figure 7. Variations in ΔX over Huancayo (HUA) on 24 December 2014 is shown with blue colored line in panels a and b similar to Figure 5d. Variation in IMF By (in red) and IMF Bz (in magenta) are superimposed on the variations ΔX in panels a and b, respectively. The intervals II and III are also marked similar to Figure 3.